J. Fluid Mech. (1995), *vol.* 288, *pp.* 59–73

On the neutral curve of the flat-plate boundary layer: comparison between experiment, Orr–Sommerfeld theory and asymptotic theory

By J. J. HEALEY

Department of Engineering, University of Cambridge, Trumpington Street, Cambridge CB2 1PZ, UK

(Received 5 July 1994 and in revised form 21 November 1994)

The neutral stability curve for the flat-plate boundary layer has been calculated using the Orr–Sommerfeld equation and compared to those obtained using upper- and lower-branch scalings. The Orr–Sommerfeld results agree well with the lower-branch scaling at Reynolds numbers relevant to experiment, but agree well with the upper-branch scaling only for $R_\delta > 10^5$. It is shown that the critical layer only emerges from the viscous wall layer when $R_\delta > 10^5$. This suggests that for $R_\delta < 10^5$, when the critical layer lies within the viscous wall layer, the disturbance has a triple-deck structure, even for the upper branch of the neutral curve (which can be reached if the phase jump across the critical layer is retained).

The transition from a triple-deck to a five-deck structure with increasing Reynolds number on the upper branch occurs relatively abruptly and can be associated with a square-root branch point in the Tietjens function. Essentially, the lower- and upper-branch scalings pertain to two different modes, the first possessing a triple-deck structure, the second a five-deck structure. The modes are connected at the branch point, and the neutral curves of each mode join to give a single curve close to this branch point. The asymptotic expansions for the upper- and lower-branch neutral curves depend upon the analyticity of the dispersion relationship, and so the proximity of the branch point indicates where these expansions will be liable to inaccuracies. This explains the poor neutral-curve predictions made by five-deck analyses at the Reynolds numbers where transition occurs.

1. Introduction

The Orr–Sommerfeld equation has great historical significance in the study of the stability of the flat-plate boundary layer. The role of viscosity is firstly to establish the Blasius profile. This profile is then assumed not to vary significantly over distances comparable to the wavelength of wavy perturbations. In this parallel-flow assumption viscosity is ignored at leading order. Viscosity is then re-introduced in the perturbation equation. This approach, although inconsistent, is widely used since it can accurately reproduce experimental results (e.g. Ross *et al.* 1970).

Consistent asymptotic solutions to the linearized Navier–Stokes equations can be obtained in which expansions are made in inverse powers of the Reynolds number. Such solutions can be made arbitrarily accurate by increasing the Reynolds number, but it is not known *a priori* whether the solution is reliable (or even applicable) at a given finite Reynolds number. Traditionally, the answer to this question has been found by direct comparison with experiment. A brief summary of how the neutral

stability curves of the asymptotic theory and Orr–Sommerfeld theory compare with experimental data is given in §2. In §3 it is shown how the Orr–Sommerfeld theory comes into close agreement with the asymptotic theory at sufficiently large Reynolds numbers. Hultgren (1987) showed how an asymptotic theory based on the lower-branch scaling can capture the upper-branch neutral curve when a particular higher-order term is retained in the expansion. Hultgren's approach is compared to the Orr–Sommerfeld theory in §4. Also presented in this section is evidence of a branch point in the Tietjens function.

Some results from Reid (1965) are discussed in §5 concerning two asymptotic approaches to the Orr–Sommerfeld equation. One gives the triple-deck neutral curve and the other gives the five-deck neutral curve. Reid gives an inequality that determines when each approach is valid. A numerical evaluation of the terms appearing in the inequality is given, and, as anticipated by Reid, it is shown how the upper branch can be obtained as a limit of the lower-branch analysis (cf. Hultgren's results). However, the lower-branch results cannot be obtained as a limit of Reid's upper-branch analysis. The effect of including small pressure gradients is shown in §6 and our conclusions are given in §7.

2. Theory and experiment

The following account is derived from the recent review by Cowley & Wu (1993), where more details can be found. Length, time, velocity and pressure will be non-dimensionalized with respect to δ, δ/U_0, U_0 and ρU_0^2 respectively where δ is the displacement thickness given by

$$\delta = 1.7208\left(\frac{x\nu}{U_0}\right)^{1/2}, \tag{1}$$

U_0 is the free-stream velocity, x is the streamwise coordinate, ρ is the density (assumed constant) and ν is the kinematic viscosity. The Reynolds number is then given by

$$R_\delta = \frac{\delta U_0}{\nu}. \tag{2}$$

Results from other papers will mostly be given in these units (this choice changes some of the familiar asymptotic scalings) or else the appropriate coordinate transformations will be provided.

For R_δ less than about 520, Orr–Sommerfeld theory predicts that all waves are damped. For larger R_δ, a band of unstable waves exists within the solid neutral curve shown in figure 1. The circles show the experimental estimates of the neutral curve obtained by Ross *et al.* (1970). Advocates of Orr–Sommerfeld theory claim that the broad agreement vindicates the parallel-flow assumption for $R_\delta > 500$. Indeed, Orr–Sommerfeld theory is often used to predict transition on aircraft wings.

The dotted line on figure 1 shows the neutral frequency predicted by the leading-order term in the asymptotic theory for the lower branch:

$$\omega \sim 0.995 R_\delta^{-1/2} \tag{3}$$

and the dashed line corresponds to the neutral curve obtained from summing the first four terms in the asymptotic expansion

$$\omega \sim 0.995 R_\delta^{-1/2}(1 + 1.597 R_\delta^{-1/4} + 10.02 R_\delta^{-1/2} + 0.988 R_\delta^{-3/4} \ln R_\delta); \tag{4}$$

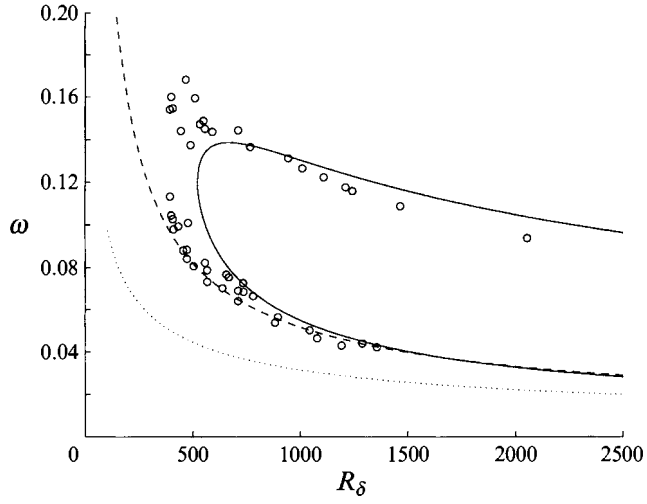

FIGURE 1. The solid line is the Orr–Sommerfeld neutral curve. Circles are experimental data from Ross *et al.* (1970). Dotted and dashed lines are the lower-branch results (3) and (4) respectively.

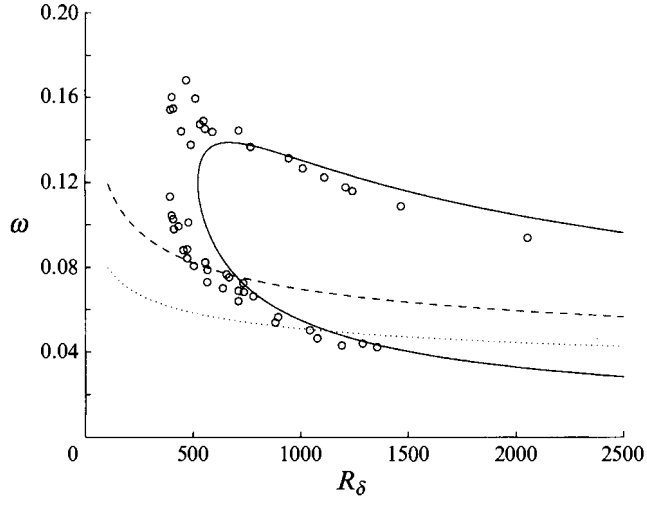

FIGURE 2. The solid line and circles are the Orr–Sommerfeld neutral curve and data from Ross *et al.* (1970) respectively. Dotted and dashed lines are the upper branch results (5) and (6) respectively.

see Smith (1979), but note that (3) and (4) are R_δ times larger than the results given by Smith owing to ω being non-dimensionalized with respect to displacement thickness (the same is also true in (5) and (6) below). There is good agreement with the experimental data. At this order, all of (4) represents a parallel-flow approximation; non-parallel effects are introduced at a still higher order. Thus for the lower branch, Orr–Sommerfeld theory, experiment and asymptotic theory are all in broad agreement.

The situation is not so clear on the upper branch. The dotted line on figure 2 is the leading-order term of the asymptotic upper-branch scaling:

$$\omega \sim 0.2027 R_\delta^{-1/5}, \tag{5}$$

and the dashed line corresponds to the neutral curve obtained from summing the first four terms in the asymptotic expansion

$$\omega \sim 0.2027 R_\delta^{-1/5}(1+0.5108 R_\delta^{-1/10}+0.3226 R_\delta^{-1/5}+0.0384 R_\delta^{-3/10}\ln R_\delta); \qquad (6)$$

see Bodonyi & Smith (1981). Again, at this order (6) represents a parallel-flow approximation. Improved agreement can be obtained by shifting the origin and replacing R_δ with $R_\delta + d$ where d is $O(1)$. This is consistent since by assumption $R_\delta \gg 1$. Bodonyi & Smith (1981) find that $d = 300$ gives better agreement for $R_\delta \sim 800$, but since this gives $d/R_\delta \approx 0.4$ such a ploy is of doubtful validity. Adding the first non-parallel terms to (6) does not bring the curves into line with either the experimental data or the Orr–Sommerfeld solution, although adding the non-parallel terms to an Orr–Sommerfeld solution gives a slight improvement (Bodonyi & Smith 1981).

If the upper branch is to coincide with the experimental data, many higher-order terms will need to be added, including non-parallel terms. This tends to suggest that non-parallel effects are important in this region of the (R_δ, ω)-plane (see the abstract of Bodonyi & Smith 1981). On the other hand, the asymptotic analyses both show that the flow is quasi-parallel at leading order, and the good performance of the Orr–Sommerfeld approximation can be attributed to this fact. Thus there is agreement between the experiment and the upper branch of the Orr–Sommerfeld calculation; and the disagreement with the upper-branch asymptotics is not easy to reconcile.

Nonetheless, at sufficiently large Reynolds number, the Orr–Sommerfeld theory ought to approach both of the parallel-flow asymptotic expansions (4) and (6). Convergence between Orr–Sommerfeld theory and the lower-branch scaling is indeed already apparent in figure 1 for $R_\delta > 1000$.

3. Numerical Orr–Sommerfeld solutions

Numerical solutions to the Orr–Sommerfeld equation have been calculated using a compound matrix method based on Davey (1982), and the neutral curves have been followed up to $R_\delta = 10^6$. The integrations were started at 6 displacement thicknesses from the wall and it was necessary to use 10000-point velocity profiles. The results are shown in figure 3 on a log–log plot. The Orr–Sommerfeld solution rapidly approaches (4), and for $R_\delta > 10^4$ is well approximated by the leading-order term in the asymptotic expansion. However, the Orr–Sommerfeld solution approaches the upper branch only for $R_\delta > 10^5$. The reason for the large delay before the upper-branch scaling is reached is that the critical layer only starts to emerge as an identifiable structure, separate from the viscous wall layer, beyond $R_\delta \approx 10^5$. This can be seen by studying the Orr–Sommerfeld eigenfunctions as the Reynolds number increases.

Figure 4(*a–h*) shows the magnitudes and phases of the eigenfunctions at $R_\delta = 3\times10^3$, 3×10^4, 3×10^5 and 10^6 for the upper-branch neutral modes. In each plot the dotted line indicates the height at which the phase velocity of the wave matches the local mean flow speed. Figures 4(*a*) and 4(*b*) show the magnitude and phase of the eigenfunction at $R_\delta = 3\times10^3$. It has the familiar form that has been measured many times in experiments, e.g. Ross *et al.* (1970). Figures 4(*c*) and 4(*d*) show the magnitude and phase at $R_\delta = 3\times10^4$; (*c*) shows a slight wobble near the dotted line but (*d*) shows nothing. Figures 4(*e*) and 4(*f*) show the magnitude and phase at $R_\delta = 3\times10^5$. A finite phase jump is beginning to form at the critical layer. Figures 4(*g*) and 4(*h*) show the magnitude and phase at $R_\delta = 10^6$. From the phase variation it is clear that the critical layer is now established. A region of almost constant phase lies above and below the critical layer with a finite jump occurring across the critical layer. The singularity in the

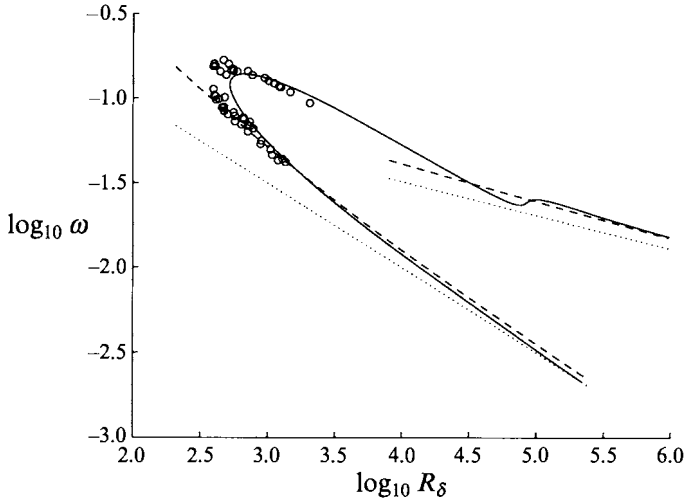

FIGURE 3. The solid line is the Orr–Sommerfeld neutral curve extended to higher Reynolds numbers. Circles are data from Ross *et al.* (1970). Dotted and dashed lines are the leading-order and four-term expansions for the upper- and lower-branch asymptotic scalings (3)–(6).

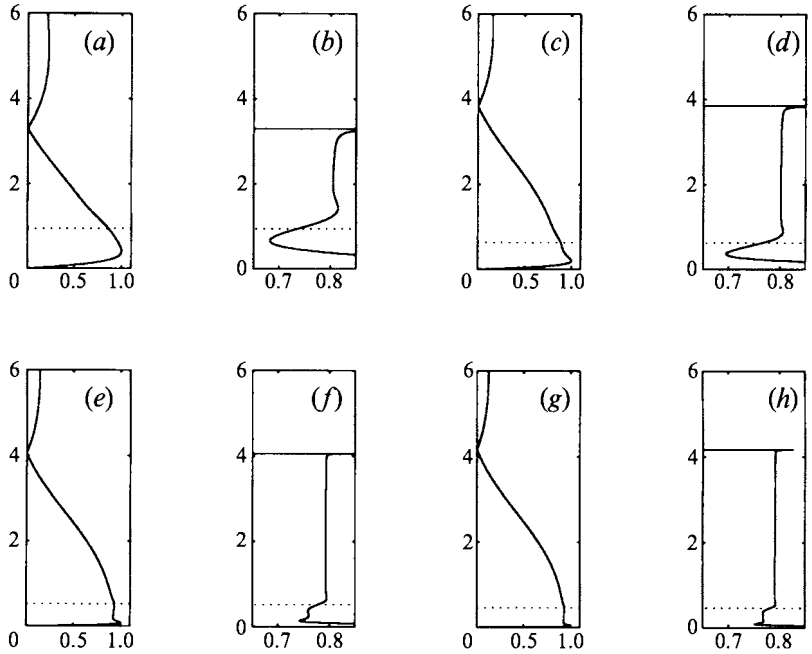

FIGURE 4. Orr–Sommerfeld eigenfunctions. (*a*, *c*, *e*, *g*) are the normalized magnitudes for $R_\delta = 3 \times 10^3$, 3×10^4, 3×10^5 and 10^6 respectively. (*b*, *d*, *f*, *h*) are the arguments in radians of the eigenfunctions for $R_\delta = 3 \times 10^3$, 3×10^4, 3×10^5 and 10^6 respectively. The dotted lines show the height at which the phase speed matches the local mean flow speed.

eigenfunction at the critical layer is logarithmic in the inviscid case and even a very small amount of viscosity is likely to lead to only a small change in the magnitude of the eigenfunction across the critical layer. Figure 4(*g*) shows that the change in the magnitude is barely discernible even at $R_\delta = 10^6$.

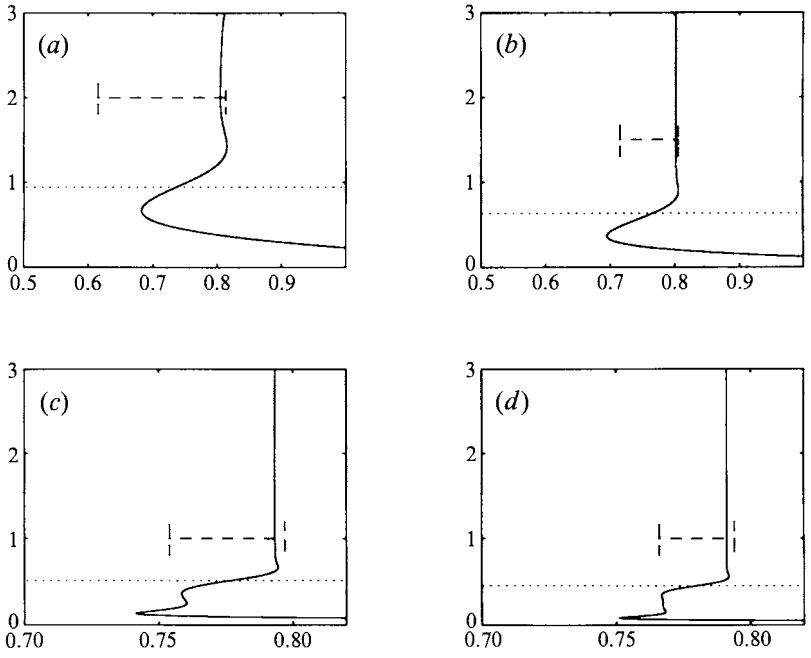

FIGURE 5. (*a–d*) The phases of the eigenfunctions for $R_\delta = 3 \times 10^3$, 3×10^4, 3×10^5 and 10^6 respectively. The bars represent the phase jump predicted by (7).

The phase jump across the critical layer is predicted by the asymptotic theory of Bodonyi & Smith (1981) and so can be compared with that observed in figures 4(*f*) and 4(*h*). The phase jump can also be conveniently extracted from the coefficient of the logarithmic term of equation (2.19) of Wu, Stewart & Cowley (1995). Converting this into standard Orr–Sommerfeld variables gives a predicted phase jump $\Delta\phi$ of

$$\Delta\phi = \left(\frac{\omega}{2\lambda\alpha}\right)^2 \left(\frac{R_\delta}{1.7208}\right)^{1/5} \pi P_0, \tag{7}$$

where α is the wavenumber, P_0 is the pressure perturbation at the wall and $\lambda = 0.33206$ (the velocity gradient at the wall). Figure 5(*a–d*) shows the phases of the eigenfunctions at the same Reynolds numbers as figure 4(*b, d, f, g*). The horizontal bars indicate the phase jump predicted by (7). The critical layer emerges from the viscous wall layer between figure 5(*b*) and 5(*c*), and the observed phase jump is close to that predicted by (7) for figures 5(*c*) and 5(*d*). For figures 5(*a*) and 5(*b*) the critical layer lies within the viscous wall layer but (7) still gives broad agreement with the phase change across the two extrema in the phase of the eigenfunctions.

The change from a triple-deck structure to a five-deck structure is shown even more strikingly in figure 6. Figures 6(*a*) and 6(*b*) correspond to the upper and lower branches respectively. The solid lines give the height of the critical layer and the dashed lines show the heights at which the phase of the eigenfunction has turning points. When moving away from the wall on the lower branch, figure 6(*b*), first the critical layer is encountered, followed almost immediately by the first turning point of the phase of the eigenfunction. A second extremum occurs a little higher and above this point the phase is practically constant. This upper extremum gives an estimate for the edge of the viscous wall layer. The dotted line in figure 6(*b*) corresponds to the triple-deck scaling for the thickness of the viscous wall layer.

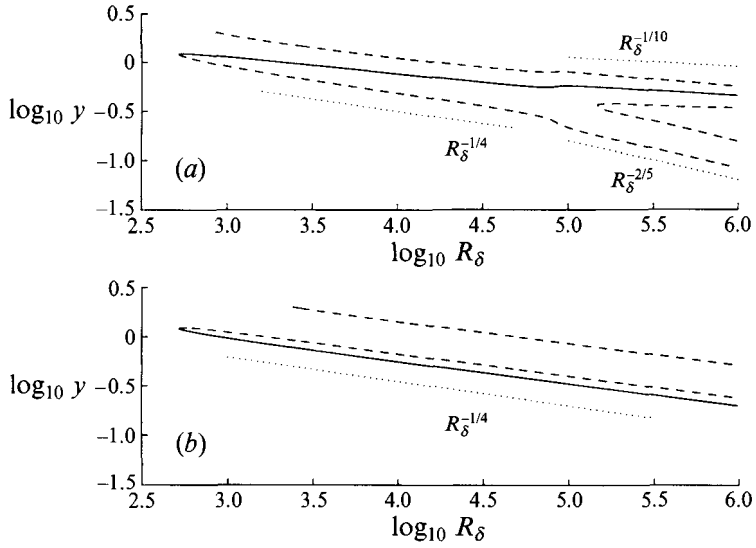

FIGURE 6. For (*a*) the upper branch and (*b*) the lower branch, the solid lines give the height of the critical layers, the dashed lines are the heights of turning points in the phase of the eigenfunction along the neutral curve, and the dotted lines show asymptotic scaling results. $R_\delta^{-1/4}$ is the height of the triple-deck viscous layer, $R_\delta^{-2/5}$ is the height of the five-deck viscous layer and $R_\delta^{-1/10}$ is the height of the critical layer.

The structure of the upper branch for $R_\delta < 10^5$ is almost identical to that of the lower branch, the thickness of the viscous wall layer even follows the triple-deck scaling. The only difference is that now the critical layer lies in between the first two extrema. As R_δ approaches 10^5 it can be seen that the critical layer gradually rises up through the viscous wall layer. For $R_\delta > 10^5$ the critical layer branches out of the viscous wall layer and the five-deck asymptotic structure is formed. The dotted lines correspond to the five-deck asymptotic scalings for the height of the critical layer and the thickness of the viscous wall layer; for $R_\delta > 10^5$ they match very well with the Orr–Sommerfeld calculations.

4. A modified triple-deck analysis

The results of the previous section suggest that for $R_\delta < 10^5$ a triple-deck structure obtains, rather than a five-deck structure. Of considerable interest, therefore, is the work of Hultgren (1987) where both upper and lower branches are calculated using a triple-deck analysis.

Hultgren obtained the following dispersion relationship:

$$\frac{\tilde{x}_1[1-F^+(\xi_0)]}{\kappa^2+\epsilon^3(\tilde{x}_1^{1/2}\kappa/2U_0'^2)\ln(-\epsilon/\kappa U_0')} = \tilde{x}_1^{3/2}-\epsilon\frac{\tilde{x}_1^{3/2}}{\kappa}(2-J_1\tilde{x}_1^{1/2}\kappa^2)+\epsilon^2\frac{\tilde{x}_1^{3/2}}{\kappa^2}(1+2J_2\tilde{x}_1^{1/2}\kappa^2+J_3\tilde{x}_1\kappa^4), \quad (8)$$

where

$$F^+(\xi_0) = 1-\mathrm{Ai}'(\xi_0)\left(\xi_0\int_{+\infty_1}^{\xi_0}\mathrm{Ai}(\xi)\,\mathrm{d}\xi\right)^{-1} \quad (9)$$

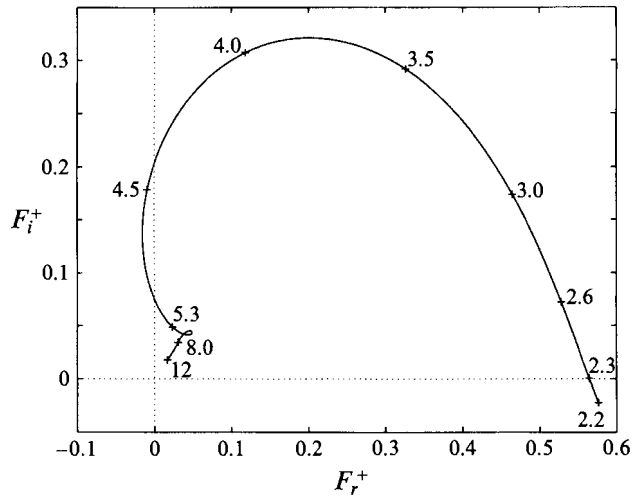

FIGURE 7. The locus of the Tietjens function $F^+(\xi_0)$ in the Argand diagram for $\xi_0 = e^{-5\pi i/6}z$, where z is real and varies between 2.2 and 12. $F^+ \to 0$ as $|\xi_0| \to \infty$ according to Reid (1965, equation (3.77)). This limit corresponds to the upper-branch scaling; $z \approx 2.3$ gives the lower-branch scaling.

is the Tietjens function, Ai is the Airy function,

$$\xi_0 = e^{-5\pi i/6}(\tilde{x}_1^{1/2}/\kappa)^{2/3}, \tag{10}$$

$$\tilde{x}_1 = 2x_1/U_0', \tag{11}$$

κ is the scaled (complex) wavenumber, x_1 is a slow streamwise coordinate, $x_1 = \epsilon^2 x$, and

$$\alpha = 1.7208\epsilon\kappa\, x_1^{1/2}, \tag{12}$$

$$R = 1.7208\, x_1^{1/2}/\epsilon^4, \tag{13}$$

$$\epsilon^6 \equiv F = \omega^* \nu / U_0^2 \ll 1, \tag{14}$$

where ω^* is the dimensional frequency. This equation is in practically the same form as equation (4.42) of Goldstein (1983). For full details concerning the derivation of (8) the reader is referred to Goldstein's paper. The constants J_1, J_2 and J_3 have the values 0.92809, -2.09322 and 1.28777 respectively, and $U_0' = 0.33206\sqrt{2}$. The $+\infty_1$ indicates that the path of integration tends to infinity in the sector $|\arg\xi| < \pi/3$.

It would be consistent to ignore the minus sign in the argument of the logarithmic term in (8) since it only contributes a complex term of $O(\epsilon^3)$ and terms of this order were neglected in the derivation of (8). However, Hultgren points out that if this 'naturally occurring normalization' is retained, then both the upper-branch and the lower-branch neutral curves can be calculated using (8). The reason for this follows from the behaviour of the Tietjens function when κ is purely real.

Figure 7 shows how $F^+(\xi_0)$ moves through the complex plane for real κ (i.e. on the neutral curve). The values on the graph itself are $\tilde{x}_1^{1/3}/\kappa^{2/3}$. For real κ the right-hand side of (8) is purely real, as is the denominator of the left-hand side if the minus sign is ignored. In this case the only solution to (8) occurs when F^+ is also real, i.e. at $\tilde{x}_1^{1/3}/\kappa^{2/3} \approx 2.3$. This root corresponds to the classical lower-branch scaling. In order to obtain the second neutral curve it is necessary for (8) to contain imaginary terms in addition to those implicit in the Tietjens function. The simplest way of achieving this is to retain the minus sign in the argument of the logarithmic term (essentially, this

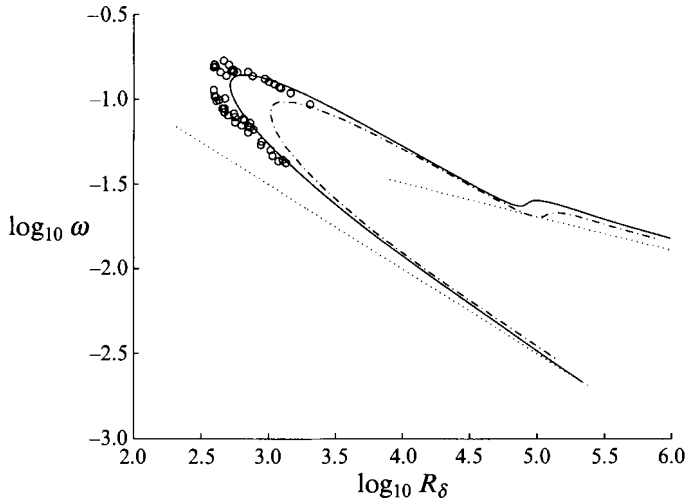

FIGURE 8. Circles are experimental results from Ross *et al.* (1970), the solid line is the Orr–Sommerfeld neutral curve and the dot–dash line is the neutral curve from (8). The dotted lines are (3) and (5).

means that the stabilizing influence of the phase jump across the critical layer is included). By using the asymptotic expansion for the Tietjens function for large $|\xi_0|$ (cf. equation (3.77) of Reid (1965), see also (18) below), the upper-branch asymptotic scaling is recovered.

Figure 8 shows a comparison between the Orr–Sommerfeld calculations of §3 and numerical solutions for the neutral curve of (8). There is excellent qualitative agreement and strong quantitative agreement over substantial ranges of R_δ. The kink in the neutral curve, beyond which the upper-branch scaling occurs, can be related to the small loop in the Tietjens function in figure 7. It is interesting to note that a similar kink was found by Reid (1965) in his approximations to the Orr–Sommerfeld equation for plane Poiseuille flow, and also for the asymptotic suction profile. These kinks were also attributed to the small loop in the Tietjens function.

Reid conjectured that this kink may not be a true feature of the full Orr–Sommerfeld equation but a consequence of the asymptotic approximations made in its evaluation. In particular, he suggests that it may disappear if the viscous correction to the inviscid solution that has a logarithmic branch point is included. The kink is apparent in our full numerical solutions to the Orr–Sommerfeld equation and also in Hultgren's triple-deck analysis. This suggest that the kink is a robust feature, which, since it follows from the Tietjens function, will be present in a wide class of stability problems.

The behaviour of the Tietjens function close to the small loop can be studied by allowing κ to become complex. Let $\xi_0 = \mathrm{e}^{-5\mathrm{i}\pi/6} z = \mathrm{e}^{-5\mathrm{i}\pi/6}(x+\mathrm{i}y)$. Figure 9 shows, on an expanded scale, loci of F^+ in the complex plane for the lines $x = \text{const.}$ and $y = \text{const.}$ The solid line is $y = 0$ and corresponds to the line in figure 7. The dotted lines are for $y = 0.1$, $y = 0.3$, $x = 6.0$ and $x = 6.3$ and the dashed lines are for $x = 6.134$ and $y = 0.161$. The latter two each form a cusp close to $z \approx 6.134 + 0.161\mathrm{i}$. This behaviour is clearly indicative of a square-root branch-point singularity at which two Riemann sheets meet. At $\xi_0 \approx (6.134+0.161\mathrm{i})\,\mathrm{e}^{-5\mathrm{i}\pi/6}$, $\mathrm{d}F^+(\xi_0)/\mathrm{d}\xi_0 \approx 0$. Comparison with (10) shows that this branch point corresponds to a slightly unstable spatial wave. However, this wavenumber only forms an eigenvalue for a complex frequency. Orr–Sommerfeld calculations show that the branch point lies off the real Reynolds number–frequency plane at a point where the imaginary part of the frequency is negative.

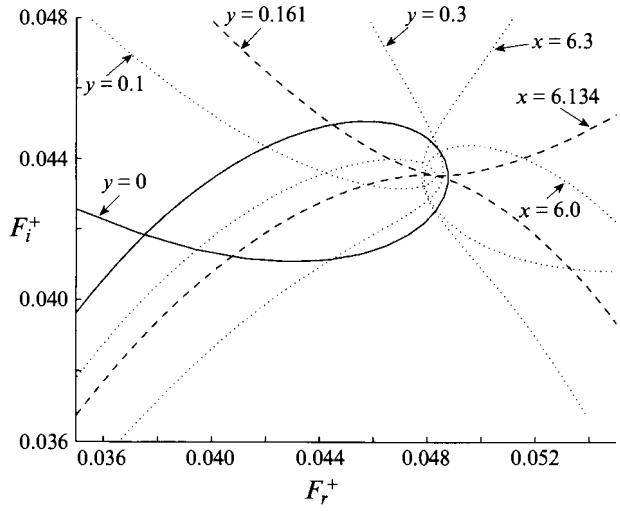

FIGURE 9. Loci of $F^+(\xi_0)$ for $\xi_0 = e^{-5\pi i/6}z = e^{-5\pi i/6}(x+iy)$ for lines $x = \text{const.}$ and $y = \text{const.}$

As mentioned earlier, the part of the Tietjens curve near $z \approx 2.3$ corresponds to the lower-branch neutral curve, while the upper-branch curve corresponds to the Tietjens function near the origin. In between these two limiting cases, the Tietjens function tightly encircles the branch point and so, in effect, switches branches near the loop. In other words, the upper branch (beyond the kink) is due to a mode with a five-deck structure, the lower branch (and the upper branch before the kink) is due to a second mode with a triple-deck structure, and the two modes join together at the branch point near the kink in the neutral curve. The close proximity of the branch point to the neutral curve means that series expansions (6) for the neutral curve will be likely to encounter inaccuracies in this region. Indeed, figure 3 confirms that the kink marks the lowest R_δ for which (6) is still a good approximation.

5. Asymptotic solutions to the Orr–Sommerfeld equation

When Hultgren obtains the upper-branch neutral curve from a triple-deck analysis, he is reproducing a result from Reid's (1965) asymptotic calculations of the Orr–Sommerfeld equation. In this context, it is useful to review briefly some of the results presented by Reid.

Reid gives two asymptotic methods for calculating the viscous solutions of the Orr–Sommerfeld equation. The first is based on the WKB method (Reid 1965, §3.2.1). The solution thus obtained is singular at the critical point, y_c. The WKB solutions are expected to be accurate except within a small neighbourhood of the critical point, i.e. when $|y-y_c| \gg |\Delta|$ where Δ is a measure of the thickness of the critical layer and is given by $\Delta = (i\alpha R_\delta U_c')^{-1/3}$ and U_c' is the velocity gradient at the critical layer.

In order for the WKB solution to give accurate eigenvalues, this inequality must hold at the boundary $y = 0$, i.e.

$$|y_c| \gg |\Delta|. \tag{15}$$

This condition is equivalent to stipulating that the critical layer must not overlap the viscous wall layer and corresponds to the five-deck asymptotic structure.

The second approach is called by Reid the 'Airy function solution' (Reid 1965, §3.2.2). This technique aims to provide a solution that is valid close to the critical layer,

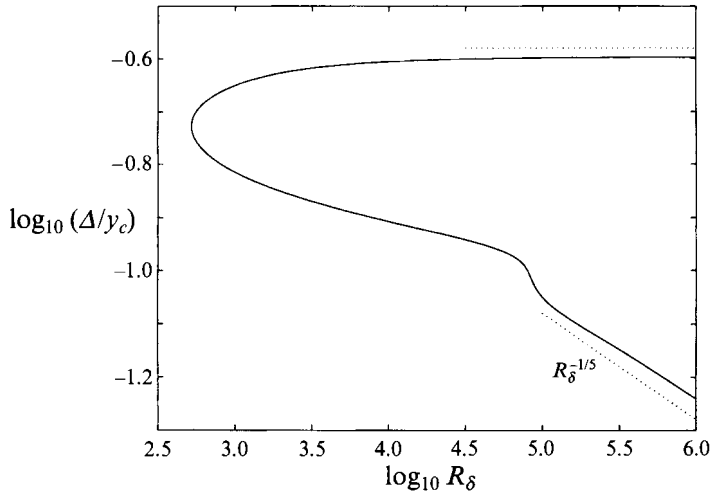

FIGURE 10. Variation of the ratio of the critical layer thickness, Δ, to the height of the critical layer, y_c, with Reynolds number. The dotted line shows the five-deck asymptotic scaling.

and involves expanding the terms in the Orr–Sommerfeld equation in powers of $(y-y_c)$. When this is done, the leading-order terms reduce to Airy's equation (with independent variable $\xi = (y-y_c)/\Delta$) and the eigenfunction is given by integrals of Airy functions. This approach is valid provided that $|y-y_c| \ll 1$. Hence the condition for accurate estimates of the eigenvalues is given by

$$|y_c| \ll 1. \tag{16}$$

The dispersion relationship is then obtained from a second viscous function, which is the Tietjens function (9).

The inequalities (15) and (16) have been investigated numerically along the neutral curve calculated in §3. As expected, y_c becomes arbitrarily small on both upper and lower branches at a sufficiently high Reynolds number, confirming that the asymptotes of both branches are accessible to the Tietjens function analysis. However, near the critical Reynolds number $y_c \sim 1.2$ and this explains the inaccuracies of (8) in this region. (The critical Reynolds number of (8) is too large by a factor of two.) The ratio Δ/y_c is plotted in figure 10. As expected, this ratio becomes arbitrarily small on the upper branch at high Reynolds numbers. However, it only follows the asymptotic scaling beyond the kink and it becomes significantly larger near the kink. It continues to increase monotonically along the neutral curve around the 'nose' and tends to a finite value along the lower branch. Reid (1965, equation (3.124)) shows that the WKB method gives the wrong leading-order scaling for the lower branch.

The Airy function (triple-deck) approach contains both the upper branch and lower branch as limiting cases, since the large-argument expansions of both viscous functions are the same to leading order:

$$G(z) = \frac{e^{i\pi/4}}{z^{3/2}}\left(1+\frac{5}{4}\frac{e^{i\pi/4}}{z^{3/2}}+\frac{25}{16}\frac{e^{i\pi/2}}{z^3}+\cdots\right), \tag{17}$$

and

$$F^+(z) = \frac{e^{i\pi/4}}{z^{3/2}}\left(1+\frac{5}{4}\frac{e^{i\pi/4}}{z^{3/2}}+\frac{151}{32}\frac{e^{i\pi/2}}{z^3}+\cdots\right) \tag{18}$$

in the limit $|z|\to\infty$, see Reid (1965, equations (3.56) and (3.77)). However, the viscous

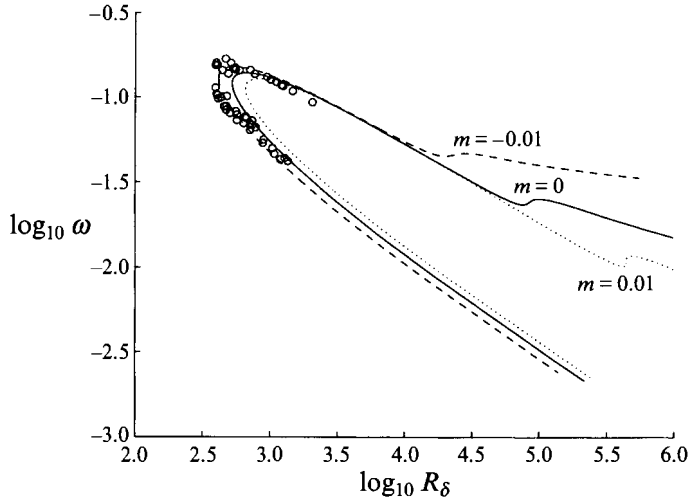

FIGURE 11. Neutral curves for Orr–Sommerfeld calculations on Falkner–Skan profiles. Circles are experimental data from Ross *et al.* (1970).

function G cannot be used for the lower branch. In fact, it does not give the kink in the neutral curve on the upper branch; this suggests that the kink represents the limit of applicability of an upper branch analysis based on the viscous function G.

6. Falkner–Skan profiles

The results of the previous sections suggest that the five-deck structure is not relevant for the Reynolds numbers at which transition actually occurs for a Blasius profile. However, for the case of an inflectional profile it may be much more important. With this in mind, we have repeated the Orr–Sommerfeld calculations for Falkner–Skan profiles under both positive and negative pressure gradients.

The similarity equation

$$2f''' + ff'' + \frac{m}{m+1}(1 - f'^2) = 0, \tag{19}$$

to be solved subject to the boundary conditions $f(0) = f'(0) = f'(\infty) - 1 = 0$ where $f' = U$, gives a profile due to a flow whose free-stream velocity is proportional to x^m. Figure 11 shows how the neutral curves vary for small variations in the pressure-gradient parameter m. The solid line is for the Blasius profile $m = 0$, the dotted line is for the favourable pressure gradient with $m = 0.01$ and the dashed line is for the adverse pressure gradient with $m = -0.01$. The latter curve passes much closer to the experimental data of Ross *et al.* (1970) than does our Blasius neutral curve, which might imply that those data were actually acquired in an adverse-pressure-gradient flow, despite intense efforts of the investigators to eliminate all influences causing pressure gradients. In fact, Saric (1990) suggests that the lowest Reynolds numbers results of Ross may have been acquired in the adverse-pressure-gradient recovery zone of the leading edge. The work of Klingmann *et al.* (1993) shows how important leading-edge conditions can be in experimental attempts to measure the neutral curve near the nose, and they obtain data that lie much closer to the Orr–Sommerfeld neutral curves.

The main point, though, is that the position of the kink on the neutral curve is very sensitive to small changes in the pressure gradient. As expected from asymptotic theory, the non-zero pressure-gradient profiles have a neutral curve that scales differently from that of the Blasius profile on the upper branch, but only beyond the kink. In particular, for the adverse-pressure-gradient profiles (which are inflectional) the five-deck critical-layer structure will indeed be relevant at much lower Reynolds numbers.

7. Conclusions

Triple-deck modes have a critical layer that lies within the viscous wall layer and five-deck modes have a critical layer that is separate from the viscous wall layer. In the latter case the phase jump across the critical layer plays a determining role in the stability, but it is neglected in the leading-order triple-deck analysis. Hultgren (1987) shows that if the phase jump is retained in the triple-deck calculation then the upper-branch neutral curve can also be obtained, including its asymptotic scaling (cf. Reid 1965).

The numerical solutions of the Orr–Sommerfeld equation presented in this paper show firstly that the critical layer lies within the viscous wall layer for the whole of the lower branch and this probably explains the success of the triple-deck analysis even near the critical Reynolds number. Secondly, on the upper branch, the critical layer is found to emerge from the viscous wall layer only at $R_\delta \approx 10^5$. Even at a free-stream velocity of 250 m s^{-1} (when compressibility effects will already be becoming important) this Reynolds number is only reached some 200 m from the leading edge. For $R_\delta < 10^5$ on the upper branch, the viscous wall layer, which contains the critical layer, scales according to the triple-deck asymptotic theory. For $R_\delta > 10^5$ the viscous wall layer and the height and thickness of the critical layer are all found to follow the five-deck asymptotic scalings.

The phase jump is an essential feature of the five-deck analysis, but it can be incorporated into the triple-deck analysis giving a theory for the whole of the unstable region, see Hultgren (1987). Indeed, given the apparent triple-deck structure of the eigenfunctions on the upper branch for $R_\delta < 10^5$, such a theory would seem to be most appropriate. At present it is not known how the five-deck analysis might be extended to make it valid for $R_\delta < 10^5$. It seems that present five-deck analyses may not be applicable to transitional Reynolds numbers. This suggests that the results of nonlinear analyses based on the upper-branch scaling, which include resonant triad interactions and nonlinear critical layer effects, may need re-appraising.

The transition from a triple-deck structure to a five-deck structure occurs relatively abruptly and is seen as a kink in the neutral curve. The kink can be traced to a small loop in the Tietjens function which encloses a square-root-singularity branch point. The asymptotic expansions (4) and (6) depend upon assuming that the dispersion relationship is analytic. At the branch point this is not true and neither series can adequately describe the dispersion relationship in this region.

The small adverse pressure gradient corresponding to a Falkner–Skan parameter of $m = -0.01$ brings the emergence of the critical-layer structure down to about $R_\delta \approx 3 \times 10^4$, which corresponds to 20 m from the leading edge of the wing of an aircraft in flight. Adverse pressure gradients tend to destabilize the flow and it is not yet clear whether a laminar flow can be maintained under an adverse pressure gradient that is sufficiently strong to bring in the critical-layer structure at transitional Reynolds numbers.

It is sometimes argued, e.g. Goldstein & Durbin (1986), that the upper-branch behaviour is more important than that for the lower branch. The argument runs as follows. The upper branch occurs at $R_\delta = O(\epsilon^{-5})$ and the lower branch is at $R_\delta = O(\epsilon^{-4})$. Since $\epsilon^{-5} \gg \epsilon^{-4}$ as $\epsilon \to 0$, the upper branch applies over a much greater range of Reynolds numbers. The lower-branch scaling can then be thought of as an 'inner' or boundary layer region for the main unstable region. In addition, nonlinear effects of initially small-amplitude disturbances will become important near the upper branch first, because this is where the amplitude is greatest. This interpretation is entirely consistent with the results presented here, but can only be applied at sufficiently high Reynolds number ($R_\delta \gg 10^5$). For transitional Reynolds numbers, the triple-deck structure prevails.

In the light of these observations it could be argued that the upper-branch scaling of Bodonyi & Smith (1981) fails to coincide with Orr–Sommerfeld predictions and experiment because of its failure to negotiate the branch point accurately. Higher-order terms, or a clever re-ordering of terms, may ultimately model the behaviour near the branch point and hence improve the agreement near the experimental data. In other words, higher-order terms are needed in the expansions because of the branch point and not because of non-parallel effects.

A cautionary note should also be registered concerning nonlinear analyses developed from the leading-order term of an asymptotic expansion that applies only at high Reynolds numbers (see also Cowley & Wu 1993). For example, Hall & Smith (1982) calculated the Landau constant for a forced plane Poiseuille flow based on the leading-order neutral curve for the lower branch, which is some way off from the Orr–Sommerfeld neutral curve (figure 2 of their paper). Notwithstanding the footnote on p. 256 of Hall & Smith, A. Davey (1983, private communication) reports that, for Reynolds numbers $< 10^6$, the sign of the Landau constant based on Orr–Sommerfeld calculations differs from that quoted by Hall & Smith, Agreement comes only at a yet higher Reynolds numbers suggesting that more terms need to be included in the neutral curve asymptotics if results are to be obtained that can be compared with experiments.

I am grateful to Professor M. Gaster FRS for making available his Orr–Sommerfeld solver. This work has benefitted from discussions with Professor Gaster and Dr S. J. Cowley and was supported by the Engineering and Physical Sciences Research Council of the UK under its Applied Nonlinear Mathematics Initiative.

REFERENCES

Bodonyi, R. J. & Smith, F. T. 1981 *Proc. R. Soc. Lond.* A **375**, 65–92.

Cowley, S. J. & Wu, X. 1993 Special course on progress in transition modelling. *AGARD Rep.* 793.

Davey, A. 1982 In *Stability in the Mechanics of Continua* (ed. F. H. Schroeder), pp. 365–372. Springer.

Goldstein, M. E. 1983 *J. Fluid Mech.* **127**, 59–81.

Goldstein, M. E. & Durbin, P. A. 1986 *Phys. Fluids* **29**, 2344–2345.

Hall, P. & Smith, F. T. 1982 *Stud. Appl. Maths* **66**, 241–265.

Hultgren, L. S. 1987 *Phys. Fluids* **30**, 2947–2951.

Klingmann, B. G. B., Boiko, A. V., Westin, K. J. A., Kozlov, V. V. & Alfredsson, P. H. 1993 *Eur. J. Mech.* B/*Fluids* **12**, 493–514.

Reid, W. H. 1965 In *Basic Developments in Fluid Dynamics*, vol. I (ed. M. Holt), pp. 249–307. Academic.

Ross, J. A., Barnes, F. H., Burnes, J. G. & Ross, M. A. S. 1970 *J. Fluid Mech.* **43**, 819–832.

SARIC, W. S. 1990 In *Instability and Transition*, vol. I (ed. M. Y. Hussaini & R. G. Voigt), pp. 162–174. Springer.

SMITH, F. T. 1979 *Proc. R. Soc. Lond.* A **366**, 91–109.

WU, X., STEWART, P. A. & COWLEY, S. J. 1995 On the weakly nonlinear development of Tollmien–Schlicting wavetrains in boundary layers. *J. Fluid Mech.* (to appear).